https://doi.org/10.5194/egusphere-2026-5685
Preprint. Discussion started: 11 November 2026
© Author(s) 2026. CC BY 4.0 License.

Beyond stomata: Interspecific heterogeneity and structural controls of urban ozone deposition

Wen Dong [a,1], Xingbao Wang [a,1], Kai Xu [a], Hanxing Zhou [a], Yincheng Huang [a], Zhi Lou [a], Yue Zhang [a], Zhenyang Huang [a], Jing Zhang [a], Junjiong Shao [a], Yuanyuan Du [b], Xiaoai Jin [a], Jian Chen [a, c], and Yuan Ren [a, c*]

[a] *College of Forestry (College of Life Sciences), Zhejiang A&F University, Hangzhou, 311300, PR China*

[b] *Huaxin Design Group Co., Ltd, Wuxi, 214100, PR China*

[c] *Tianmushan Forest Ecosystem Orientation Observation and Research Station of Zhejiang Province, Hangzhou, 311300, PR China*

[1]These authors contributed equally to this work.

*Corresponding Author:

College of Forestry (College of Life Sciences), Zhejiang A&F University, 666 Wusu Street, Hangzhou 311300, PR China

E-mail: renyuan@zafu.edu.cn (YR)

https://doi.org/10.5194/egusphere-2026-5685
Preprint. Discussion started: 11 November 2026
© Author(s) 2026. CC BY 4.0 License.

ABSTRACT

Urban environments are critical ozone (O_3) hotspots where intense precursor emissions and high population densities escalate human exposure risks. Current deposition models typically rely on coarse land-use classifications, failing to capture the species-level heterogeneity at the city scale. We quantified O_3 dry deposition across 20 common tree species in a subtropical megacity using a modified micrometeorological gradient method to derive species-resolved resistance parameters. Field measurements identified substantial interspecific variation: daytime canopy concentration gradients peaked at 10.02 ± 0.86 ppb (*Platanus acerifolia*). While standardized stomatal conductance correlates with the inverted minimum stomatal resistance ($1/R_{s,\ min}$, R^2 = 0.36, P < 0.001), this relationship provides partial physiological support for the inferred resistance parameters. Sensitivity analysis showed that model-estimated deposition velocity was most sensitive to *LAI*, followed by wind speed and roughness length. Notably, a 20% LAI increase reduced estimated deposition velocity by 17.55% under the prescribed sensitivity experiments. These findings highlight species-level differences in O_3 deposition and the coupled roles of canopy structure, aerodynamic transport, and physiological regulation.The resulting resistance estimates provide observational constraints for species-resolved parameterization in atmospheric deposition models, although their transferability requires further validation.

KEYWORDS: ozone dry deposition; species-resolved parameters; canopy architecture; air-quality modeling; urban ecosystem service

https://doi.org/10.5194/egusphere-2026-5685
Preprint. Discussion started: 11 November 2026
© Author(s) 2026. CC BY 4.0 License.

1. INTRODUCTION

Tropospheric ozone (O_3) poses a persistent challenge to urban air quality management, fundamentally threatening human health, impairing plant productivity, and modulating the oxidation capacity of the atmosphere (Monks et al., 2015; Fleming et al., 2018). Unlike primary pollutants, surface O_3 is governed by complex photochemical interactions between nitrogen oxides (NOx) and volatile organic compounds (VOCs), which complicates mitigation efforts in precursor-dense urban environments (Ren et al., 2017; Ren et al., 2014). This management dilemma is particularly evident in China, where O_3 concentrations have remained recalcitrant, effectively decoupling from the successful downward trend in particulate matter observed over the past decade (Li et al., 2019; Xu et al., 2021). Given that urban centers function as the nexus of both concentrated emissions and high population densities, they endure disproportionately high risks of human exposure (Dong et al., 2026). A mechanistic understanding of O_3 removal is therefore critical to improve forecasting accuracy and inform nature-based exposure mitigation.

Urban trees are widely prioritized as a primary O_3 sink because their canopies provide expansive surfaces for dry deposition (Sicard et al., 2018; Nowak & Greenfield, 2018). Within current resistance-based frameworks, O_3 deposition is regulated by a coupling of aerodynamic transport and canopy resistance (Zhang et al., 2003; Wesely, 2007). However, most urban assessments remain coarse, typically aggregating diverse vegetation into broad land-cover categories that fail to capture street-scale heterogeneity (Grote et al., 2016; Wang et al., 2021). This homogenization is problematic because O_3 exchange is highly sensitive to species-specific traits, including canopy architecture, foliage density, and stomatal regulation (Büker et al., 2007; Fowler et al., 2009). Crucially, many regional air-quality models are unconstrained by urban-specific measurements, relying instead on empirical parameters extrapolated from rural forest ecosystems (Clifton et al., 2020; Kim et al., 2021; Baklanov et al., 2007). Such parameter borrowing ignores the unique turbulence and microclimatic forcing of urban canyons, leading to significant uncertainties in evaluating the actual O_3 mitigation

https://doi.org/10.5194/egusphere-2026-5685
Preprint. Discussion started: 11 November 2026
© Author(s) 2026. CC BY 4.0 License.

provided by heterogeneous urban forests.

Field-based evidence for O_3 deposition remains a critical bottleneck, as most previous studies focused on community-scale exchange in continuous forests rather than individual tree species in complex urban settings (Fitzky et al., 2019; Fares et al., 2020). This scale mismatch is problematic because O_3 removal is highly sensitive to species-specific traits, including canopy architecture and stomatal regulation, which vary significantly even under identical environmental conditions (Fowler et al., 2009; Stein et al., 2014; Lin et al., 2019). Existing observations often fail to decouple species-level differences in canopy resistance from short-term environmental forcing, such as variation in radiation and vapor pressure deficit (Emberson et al., 2000; Gaur & Singh, 2024). Although existing deposition models describe interactions among canopy structure, atmospheric transport, and physiological regulation, species-resolved observations remain limited for evaluating these processes in urban environments. This observational gap constrains the estimation of species-specific resistance parameters and their application in atmospheric deposition models (Manes & Salvatori, 2014).

To address these limitations, this study quantified O_3 dry deposition across 20 common urban tree species in Hangzhou, a subtropical megacity representing high-density urbanization, severe summer O_3 pollution, and diverse urban greening assemblages in eastern China. Using a modified micrometeorological gradient method under comparable summer clear-sky conditions, we measured vertical O_3 concentration gradients to estimate species-resolved deposition velocities and fluxes and derived canopy resistance within a standardized three-resistance framework (Wu et al., 2015). The specific objectives were to: (1) characterize interspecific differences in O_3 dry deposition velocity and flux; (2) estimate species-specific stomatal and non-stomatal resistance parameters and examine their relationships with measured stomatal conductance; and (3) evaluate the sensitivity of estimated deposition velocity to canopy structural and environmental parameters within the modified-gradient framework. By providing a field-constrained set of species-resolved resistance estimates, this study aims to support the evaluation and refinement of urban vegetation parameterization in

https://doi.org/10.5194/egusphere-2026-5685
Preprint. Discussion started: 11 November 2026
© Author(s) 2026. CC BY 4.0 License.

atmospheric deposition models and support species-aware urban greening strategies.

2. MATERIALS AND METHODS

2.1 Site characterization and experimental configuration

Field observations were conducted in Hangzhou (30°14′56.3″N, 120°12′18.8″E), a representative subtropical megacity in the Yangtze River Delta, China (**Figure 1**). We quantified O_3 dry deposition for 20 common urban tree species, encompassing the dominant plant functional types (PFTs) in regional greening: evergreen broadleaf (ebt), deciduous broadleaf (dbt), and evergreen needleleaf (ent) trees. Although the field experiments were conducted in Hangzhou, these target species were strategically selected based on the ecological paradigm of urban biotic homogenization. As illustrated in Figure S6, these species are widely cultivated across China, particularly dominating the urban canopies east of the demographic 'Hu Line', which encloses over 94% of the nation's population and the vast majority of its built-up urban centers. Furthermore, key taxa such as *Platanus acerifolia* and *Magnolia grandiflora* are ubiquitous street trees globally, widely planted in North American and European megacities. These species collectively represent over 70% of the regional urban canopy, ensuring the statistical weight and broad generalizability of observational matrix.[4] For each species, tree height, diameter at breast height (DBH), and crown width were recorded from three sampled individuals to calculate species-specific means (Table S1).

https://doi.org/10.5194/egusphere-2026-5685
Preprint. Discussion started: 11 November 2026
© Author(s) 2026. CC BY 4.0 License.

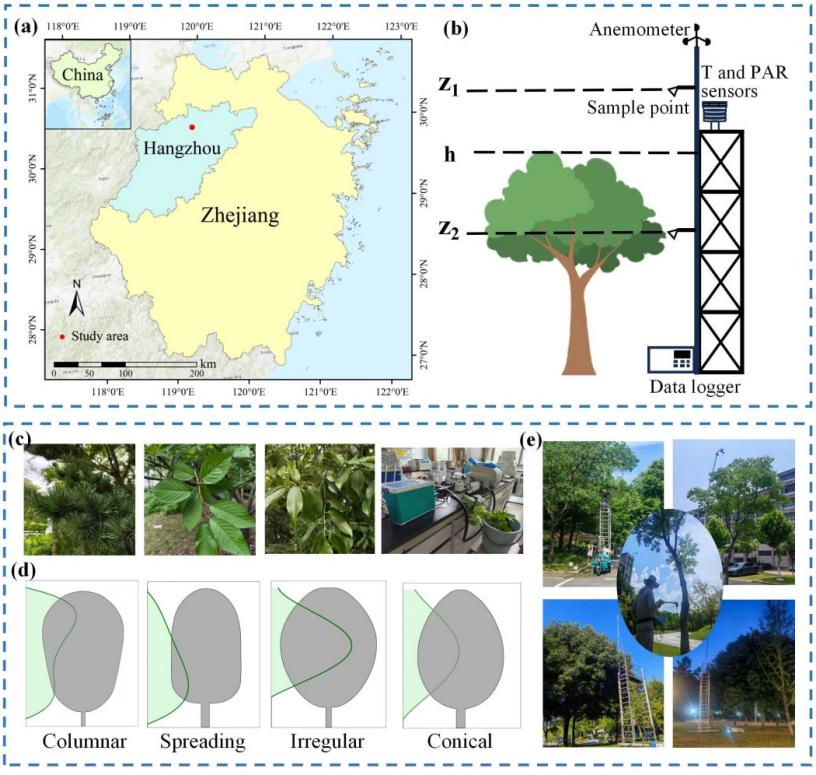


Figure 1. Schematic of the multi-dimensional observational framework and experimental design. (a) Geographic location of the study area within Hangzhou, China; (b) Vertical configuration for O_3 concentration gradient and micrometeorological flux measurements across the canopy-atmosphere interface; (c) Representation of major PFTs and leaf-level gas exchange protocol using the LI-6800 system; (d) Schematic of leaf area density (LAD) quantification across diverse canopy architectures (**Text S1**); (e) In situ photograph of the mobile monitoring platform deployed in a representative urban street-side setting (**Text S2**).

To satisfy the fetch and homogeneity requirements for micrometeorological flux estimation, each target species was represented by a large, mature, single-species canopy patch. Instruments were deployed on a stable mobile platform with an adjustable telescopic mast reaching up to 14 m. To mitigate building-induced airflow

https://doi.org/10.5194/egusphere-2026-5685
Preprint. Discussion started: 11 November 2026
© Author(s) 2026. CC BY 4.0 License.

distortion, observations were only retained when the horizontal distance from adjacent structures exceeded five times the building height (Schmid, 2002; Britter & Hanna, 2003). Furthermore, data analysis was limited to periods when the prevailing wind originated from the target canopy fetch. All measurements were performed during the summer growing season (July–September) under stable clear-sky conditions. Each species was characterized through three independent full-diurnal observation cycles (24 h), providing robust replication while maintaining the spatial comparability necessary for canopy-scale flux analysis.

2.2 Vertical O_3 profiling and ancillary observations

Vertical O_3 concentration gradients were resolved using a synchronized dual-height sampling system. Two UV photometric analyzers (Thermo Scientific 49i, USA) were deployed on a telescopic mobile platform (adjustable up to 14 m) to capture concentrations at two levels: a reference height above the canopy (z_1) and an intra-canopy height (z_2) (**Figure 1b**). To eliminate potential systematic offsets between instruments, a periodic analyzer rotation protocol was strictly implemented across the replicates. This cross-calibration ensured that the resolved vertical differentials accurately reflected the concentration drop induced by canopy-level uptake rather than instrumental artifacts.

Simultaneous environmental characterization was conducted alongside the O_3 observations. Three-dimensional wind components and direction were monitored via an ultrasonic anemometer at the reference height. Air temperature (T_a) and relative humidity (RH) were recorded in close proximity to the O_3 inlets (Winsen WHT 30, China), while solar irradiance was tracked continuously to resolve photochemical drivers. Canopy-scale structural metrics, specifically the Leaf Area Index (LAI), were quantified beneath each target canopy using a plant canopy analyzer (TOP-1300, China). Vapor pressure deficit (VPD) was subsequently derived from T_a and RH. To align canopy-scale behavior with leaf-level physiology, stomatal conductance (g_s) was measured in situ using a portable gas exchange system (LI-6800, LI-COR Biosciences,

https://doi.org/10.5194/egusphere-2026-5685
Preprint. Discussion started: 11 November 2026
© Author(s) 2026. CC BY 4.0 License.

USA) under standardized chamber conditions (ambient CO_2, saturated *PAR*, and controlled leaf temperature).

2.3 Ozone dry deposition and resistance parameterization

2.3.1. Quantification of O_3 flux and deposition velocity

Ozone dry deposition flux (F_d) was estimated using the modified gradient method (MGM) (Wu et al., 2015). Relative to the conventional gradient approaches, the MGM integrates concentration differentials across the canopy-atmosphere interface, significantly improving flux estimation accuracy in structurally heterogeneous urban canopies. Assuming atmospheric turbulence as a molecular diffusion process, the vertical exchange is governed by the flux-gradient relationship (Baldocchi et al., 1988):

$$F(z) = -K_c(z)\frac{dC}{dz} \quad (1)$$

where $K_c(z)$ is the vertical eddy diffusivity coefficient and dC/dz represents the vertical concentration gradient.

Based on the constant flux layer assumption above the canopy (Wesely et al., 2007), we incorporated concentrations at the reference height (z_1) and intra-canopy height (z_2) to derive the net flux (F):

$$F = -\frac{C_1 - C_2}{R_a(z_1{:}\,h) + R_a(h{:}\,z_2)} \quad (2)$$

where C_1 and C_2 are the measured O_3 concentrations at z_1 and z_2, respectively, and R_a is the aerodynamic resistance across the respective layers. The dry deposition velocity (V_d) was subsequently calculated as:

$$V_d = -F/C_1 \quad (3)$$

Detailed derivations of the height-integrated R_a and the MGM framework are provided in **Text S3**.

2.3.2 Resistance modeling and canopy characterization

To isolate the biological and structural drivers of deposition (Zhang et al., 2003), V_d was decomposed using the classical three-resistance analogy:

https://doi.org/10.5194/egusphere-2026-5685
Preprint. Discussion started: 11 November 2026
© Author(s) 2026. CC BY 4.0 License.

$$R_c = V_d^{-1} - R_a - R_b \quad (4)$$

where R_a and R_b represent the aerodynamic resistance and quasi-laminar boundary-layer resistance, respectively. R_a was estimated using Monin-Obukhov similarity theory, while R_b was determined from friction velocity and the molecular diffusivity of O_3 in air. The specific parameterizations for R_b and the temperature-dependent diffusion coefficients follow standard micrometeorological formulations, as detailed in **Text S3**.

In this study, R_c was treated as an integrated apparent resistance rather than an environment-independent constant. This term integrates both stomatal and non-stomatal pathways and remains sensitive to short-term environmental forcing. Consequently, R_c serves as a comparative canopy-scale indicator of interspecific deposition performance within our unified observational framework.

2.4 Resistance decomposition and inversion of intrinsic parameters

To decouple intrinsic biological capacity from short-term environmental forcing and facilitate interspecific comparisons (Wesely et al., 2002), the observed apparent canopy resistance (R_c) was further decomposed into stomatal resistance (R_s) and non-stomatal resistance (R_{ns}) using a parallel-resistance framework:

$$R_c^{-1} = R_s^{-1} + R_{ns}^{-1} \quad (5)$$

The stomatal component R_s was parameterized as a function of the minimum stomatal resistance ($R_{s,min}$) and a series of multiplicative environmental response functions:

$$R_s(t) = R_{s,min}[f_1(t) \cdot f_2(t) \cdot f_3(t) \cdot f_4(t)]^{-1} \quad (6)$$

where f_1–f_4 are dimensionless functions representing the physiological constraints of solar irradiance, soil moisture, vapor pressure deficit, and air temperature, respectively. The specific mathematical formulations and empirical response coefficients for these functions are detailed in Text S4 of the Supporting Information.

For each species, the intrinsic parameters $R_{s,min}$ and R_{ns} were estimated from the full-diurnal time series using nonlinear least-squares fitting. This inversion process was conducted by minimizing the residual sum of squares between the observed apparent

https://doi.org/10.5194/egusphere-2026-5685
Preprint. Discussion started: 11 November 2026
© Author(s) 2026. CC BY 4.0 License.

canopy resistance ($R_{c,obs}$) and the modeled values ($R_{c,mod}$). To ensure physiological and physical consistency, the optimization was restricted to daytime periods with positive solar irradiance, and both calibrated parameters were constrained to positive domains within the resistance-analogy framework.

2.5 Sensitivity and statistical analyses

A univariate sensitivity analysis was conducted to quantify the response of model-estimated V_d to fluctuations in key environmental and structural input parameters. Specifically, air temperature (T), wind speed (u), leaf area index (LAI), leaf area density (LAD), and roughness length (z_0) were each perturbed by ± 20% relative to the baseline condition, while the remaining variables were held constant. The resulting changes in V_d relative to the baseline were used to evaluate the sensitivity of the modified-gradient estimation framework to individual input parameters and their diurnal variation. These responses represent sensitivities within the estimation framework rather than independently observed effects on O_3 deposition.

For each tree species, observations from three sampled individuals were treated as independent biological replicates. Interspecific differences in V_d, F, ΔC, and R_c were evaluated using one-way Analysis of Variance (ANOVA), followed by Tukey's Honestly Significant Difference (HSD) post-hoc test for multiple comparisons. Statistical significance was defined at $P < 0.05$, with distinct lowercase letters used to denote significant differences in the figures. The relationship between measured leaf-level stomatal conductance (g_s) and the inverse of inferred minimum stomatal resistance ($1/R_{s,min}$)was assessed using linear regression based on paired tree-level observations. All results are presented as means ± standard errors (SE).

3. RESULTS

3.1 Temporal dynamics of O_3 deposition velocity across species

All studied species exhibited pronounced and consistent diurnal variation in V_d, strictly synchronized with the solar radiation cycle (**Figure 2**). Typically, V_d values

https://doi.org/10.5194/egusphere-2026-5685
Preprint. Discussion started: 11 November 2026
© Author(s) 2026. CC BY 4.0 License.

remained at a nocturnal baseline, escalated rapidly following sunrise, reached daytime maxima between late morning and early afternoon, and subsequently attenuated as irradiance diminished. Despite this shared fundamental rhythm, the magnitude and temporal structure of peak deposition differed substantially among the 20 species.

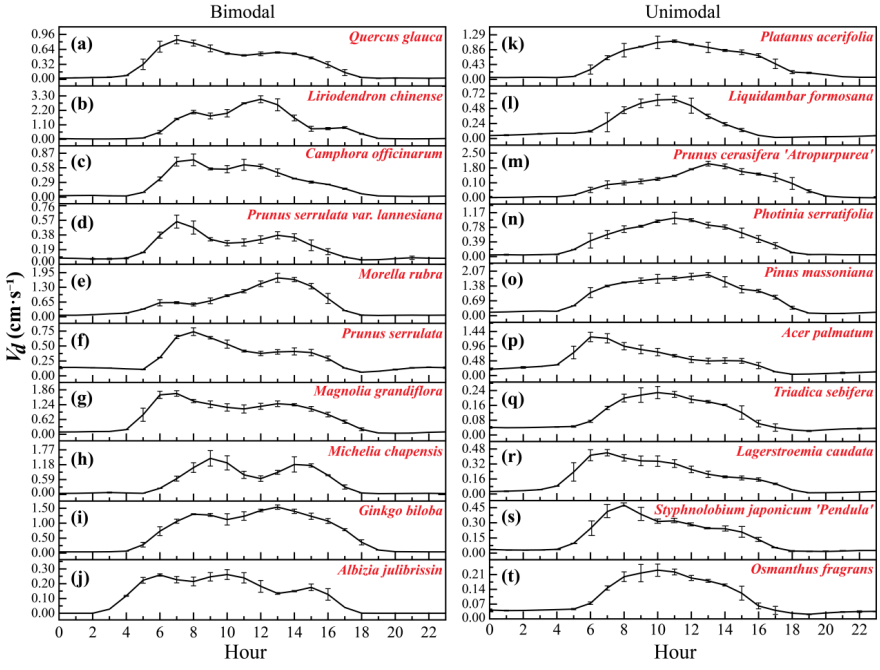


Figure 2. Interspecific heterogeneity in the diurnal profiles of O_3 deposition velocity (V_d) across 20 urban tree species. (a-j) Species exhibiting bimodal deposition patterns; (k-t) Species exhibiting unimodal or midday-plateau patterns. Each panel presents species-level means (solid lines) with shaded error bars representing SE (n = 3).

Two distinct temporal modalities emerged from the diurnal profiles. A bimodal pattern, characterized by dual peaks in the morning and afternoon with a slight midday depression, was prominently observed in species such as *Quercus glauca* and *Liriodendron chinense* (**Figure 2**a-j). This modality potentially reflects peak stomatal opening during high-light periods interrupted by midday stomatal regulation. Conversely, a unimodal or midday-plateau pattern was identified in species like

https://doi.org/10.5194/egusphere-2026-5685
Preprint. Discussion started: 11 November 2026
© Author(s) 2026. CC BY 4.0 License.

Platanus acerifolia and *Liquidambar formosana*, where deposition efficiency was maintained at elevated levels throughout the central daylight hours (**Figure 2**k-t).

Interspecific heterogeneity was further evident in the intensity and sensitivity of the deposition response. *L. chinense* and *P. cerasifera* exhibited the highest instantaneous V_d values among the cohort, while *Osmanthus fragrans* displayed the most conservative deposition capacity, marked by minimal peak values and a restricted diurnal amplitude. Furthermore, deciduous broadleaf species generally demonstrated a more rapid morning escalation to peak V_d, whereas evergreen species exhibited smoother temporal transitions, reflecting potential differences in the physiological response times of their canopy conductance to environmental drivers.

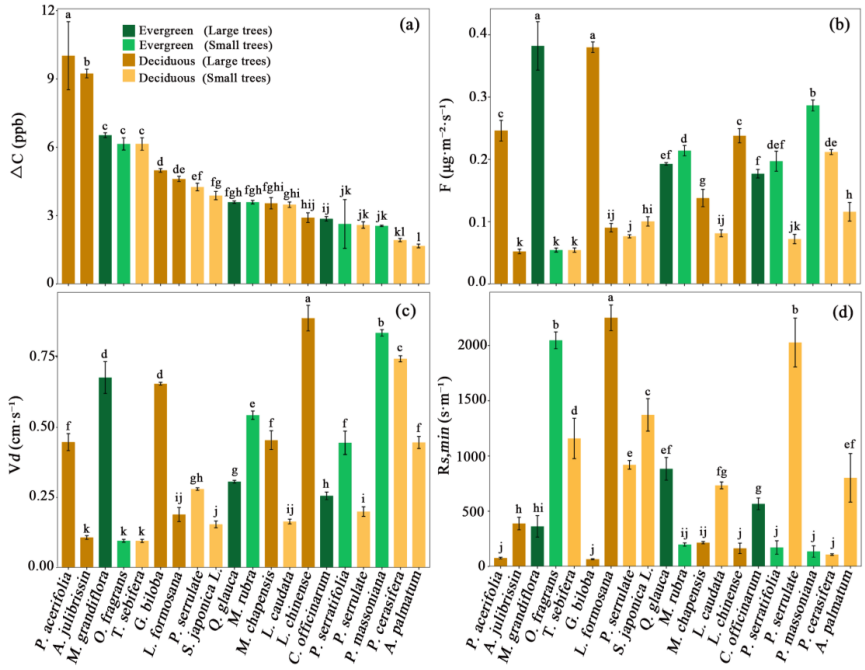


Figure 3. Comparative analysis of O_3 deposition metrics across 20 urban tree species. (a) Mean canopy concentration differentials (ΔC), (b) O_3 dry deposition flux (F), (c) O_3 dry deposition velocity (V_d), and (d) Inverted minimum stomatal resistance ($R_{s,min}$). Error bars represent species-level means ± SE (n=3). Different lowercase letters indicate significant differences among species ($P < 0.05$).

https://doi.org/10.5194/egusphere-2026-5685
Preprint. Discussion started: 11 November 2026
© Author(s) 2026. CC BY 4.0 License.

3.2 Interspecific heterogeneity in ΔC, V_d, F, and $R_{s,min}$

One-way ANOVA revealed significant interspecific differences across all quantified deposition metrics ($P < 0.05$; **Figure 3**). Across the 20-species cohort, O_3 concentrations were consistently higher at the above-canopy reference height (z_1) than within the canopy (z_2), confirming the canopy's role as a persistent O_3 sink (Fig. 3a). The vertical concentration gradient (ΔC) exhibited marked variation among species, with the highest mean value in *P. acerifolia* (10.02 ± 0.86 ppb), followed by *Albizia julibrissin* (9.24 ± 0.11 ppb).

Although both V_d and F varied substantially among species, their respective rankings were not identical, reflecting a decoupling between deposition efficiency and total mass transfer (**Figure 3**b-c). *L. chinense* exhibited the highest mean daytime V_d (0.890 ± 0.026 cm s^{-1}), whereas the highest mean daytime F was observed in *Magnolia grandiflora* (0.382 ± 0.022 μg m^{-2} s^{-1}).

Significant interspecific variation was also resolved in the minimum stomatal resistance ($R_{s,min}$), the key intrinsic parameter derived from our inversion framework (**Figure 3**d). These results indicate that normalized stomatal constraints differ fundamentally across urban tree functional types. Collectively, the simultaneous expression of species-specific signals in concentration gradients, deposition performance, and intrinsic resistance parameters underscores the necessity of species-resolved approaches in urban air-quality assessments.

3.3 Physiological linkage between standardized g_s and inverted $1/R_{s,min}$

Across the tree-level observational cohort, a statistically significant positive linear relationship was resolved between standardized g_s and $1/R_{s,min}$ ($P<0.001$; **Figure 4**). As standardized g_s increased, the inverted minimum stomatal resistance ($1/R_{s,min}$) exhibited a corresponding escalation, with the regression model yielding a moderate explanatory power (R^2 = 0.36). This result confirms that species or individual observations characterized by higher gas-exchange capacity under standardized conditions generally maintain lower intrinsic stomatal constraints.

https://doi.org/10.5194/egusphere-2026-5685
Preprint. Discussion started: 11 November 2026
© Author(s) 2026. CC BY 4.0 License.

The distribution within the species-level parameter space, however, exhibited notable non-uniformity. The upper envelope of the scatterplot was primarily defined by six high-leverage observations from *Ginkgo biloba* and *P. acerifolia*, both of which integrated high standardized g_s with elevated $1/R_{s,min}$ values. These specific data points contributed substantially to the overall positive regression trend. In contrast, the majority of the remaining species clustered within the lower-to-middle regions of the plot, exhibiting a more restricted range of $1/R_{s,min}$. Several species exhibited stochastic deviations from the fitted regression line, indicating that while standardized g_s serves as a primary physiological driver, it does not fully account for the total interspecific variance in $R_{s,min}$.

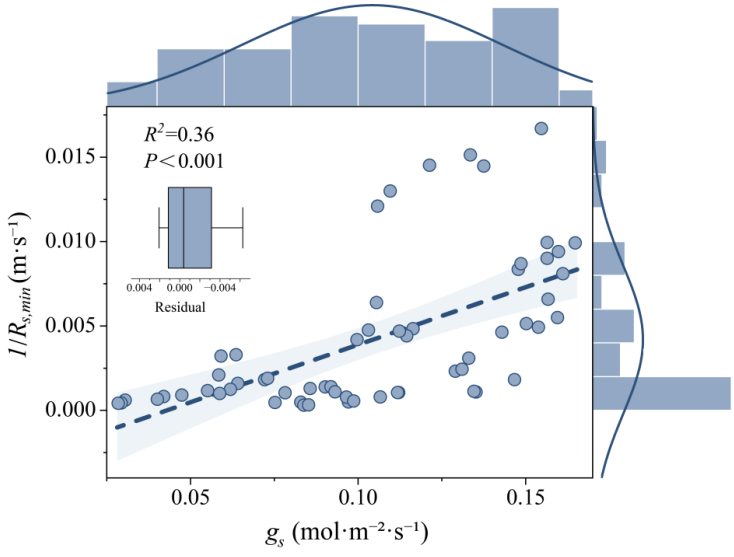


Figure 4. Physiological coupling between standardized stomatal conductance (g_s) and inverted minimum stomatal resistance ($1/R_{s,min}$) across tree-level observations. The main panel illustrates the fitted linear regression with 95% confidence interval; the top and right panels show marginal distributions, and the inset shows residuals.

3.4 Sensitivity of V_d to environmental and structural drivers

Univariate sensitivity analysis revealed distinct hierarchies and temporal profiles in the response of model-estimated V_d to perturbations in major environmental and

https://doi.org/10.5194/egusphere-2026-5685
Preprint. Discussion started: 11 November 2026
© Author(s) 2026. CC BY 4.0 License.

structural parameters (**Figure 5**). Based on the integrated daily mean response, the relative model sensitivity of the tested factors was ranked as: $LAI > u > z_0 > LAD \approx T$. Among these factors, *LAI* produced the largest and most temporally consistent response in V_d. Specifically, a 20% decrease in *LAI* resulted in an average V_d increase of 21.07%, whereas a 20% increase in LAI reduced the estimated V_d by 17.55%. Wind speed (u) showed the second-largest sensitivity, with mean V_d shifts of +20.18% and –16.66% under ±20% perturbations, respectively. Roughness length (z_0) ranked third, with corresponding changes of +12.81% and –12.46%, while *LAD* and air temperature (T) showed comparatively smaller responses on the daily mean V_d.

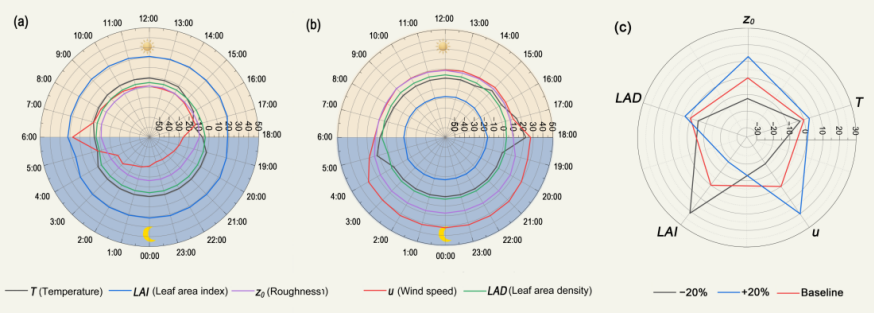


Figure 5. Sensitivity of O_3 deposition velocity (V_d) to primary environmental and structural drivers across the diurnal cycle. (a) Diurnal V_d response to +20% perturbations in individual drivers; (b) Diurnal V_d response to –20% perturbations; and (c) Comparative radar plot illustrating the overall magnitude of V_d percentage change across all tested factors.

The temporal sensitivity patterns exhibited distinct diurnal variability across different input parameters. Wind speed and roughness length produced the largest responses during the nocturnal and early morning periods. In contrast, the sensitivity of V_d to T was primarily concentrated in the late afternoon and evening; notably, a +20% perturbation in T at 18:00 resulted in a peak V_d increase of 22.38%. Unlike the meteorological variables, the sensitivity of V_d to *LAI* remained relatively stable

https://doi.org/10.5194/egusphere-2026-5685
Preprint. Discussion started: 11 November 2026
© Author(s) 2026. CC BY 4.0 License.

throughout the diurnal cycle. Under baseline conditions, V_d followed a characteristic single-peak diurnal trajectory, escalating after sunrise to a maximum of 0.91 cm s^{-1} at 13:00 before a gradual evening decline. Overall, these results indicate that the magnitude and diurnal variation of model-estimated V_d responses differ among the tested parameters.

4. DISCUSSION

4.1 Coupled mechanisms driving interspecific variability in O_3 deposition

Our results indicate that interspecific differences in urban O_3 deposition are expressed through the simultaneous coupling of canopy concentration gradients (ΔC), deposition performance (V_d and F_d), and inferred physiological parameters ($R_{s,min}$). This multi-dimensional variation suggests that evaluating urban O_3 mitigation solely through total deposition velocity or stomatal properties provides an incomplete picture of a species' actual ecological role (Fares et al., 2020). Instead, the observed patterns are consistent with a holistic resistance-based framework in which canopy-scale uptake is determined by the dynamic interaction between atmospheric transport efficiency and biological exchange capacity (Clifton et al., 2020; Karl et al., 2010). Canopy architecture influences both the distribution of available deposition surfaces and the vertical transport of O_3, while stomatal regulation determines the physiological component of canopy uptake. Multilayer deposition models further demonstrate that these processes vary vertically within the canopy, depending on the distribution of foliage, turbulence, and stomatal activity (Zhou et al., 2017). By resolving these components across 20 tree species, our results provide species-level evidence consistent with the coupled influence of canopy structure, aerodynamic transport, and physiological regulation on urban O_3 exchange..

A critical observation supporting this coupled mechanism is the functional decoupling identified among the major deposition metrics across the 20-species cohort. For instance, while *P. acerifolia* exhibited the most pronounced vertical concentration gradients (ΔC), this did not directly translate into the highest net mass flux (F_d) or

https://doi.org/10.5194/egusphere-2026-5685
Preprint. Discussion started: 11 November 2026
© Author(s) 2026. CC BY 4.0 License.

deposition velocity (V_d). This discrepancy highlights that a strong vertical gradient may reflect localized O_3 depletion under restricted atmospheric mixing rather than superior absolute sink strength. Furthermore, the substantial interspecific variation resolved in $R_{s,min}$ suggests that normalized stomatal regulation differs significantly among urban trees, yet this physiological signal does not translate linearly into total deposition performance because leaf-level exchange is modulated by canopy-scale transport and non-stomatal uptake (Wesely, 2007; Körner, 1995). Consequently, common urban trees should be treated as functionally heterogeneous surfaces rather than uniform sinks in regional air-quality assessments.

4.2 Physiological relevance and scaling of stomatal regulation

The significant positive relationship observed between standardized stomatal conductance (g_s) and the inverted minimum stomatal resistance ($1/R_{s,min}$) indicates that the calibrated resistance parameters are associated with independently measured leaf-level physiological characteristics. This agreement supports the biological relevance of the inversion framework used in this study and suggests that $R_{s,min}$ captures part of the interspecific variation in stomatal regulation,, aligning with the stomatal scaling principles (Medlyn et al., 2011). Photosynthesis-based deposition approaches explicitly couple stomatal conductance to carbon assimilation and environmental regulation, providing a more mechanistic representation of physiological controls than prescribed multiplicative response functions (Lei et al., 2020; Sun et al., 2022)..The observed relationship provides partial physiological support for the inferred parameters, although it does not independently validate the separation of stomatal and non-stomatal deposition pathways.

However, the moderate explanatory power (R^2 = 0.36) highlights the inherent complexities in scaling leaf-level gas exchange to canopy behavior within urban environments. Leaf-level conductance captures only a specific facet of stomatal function under standardized chamber conditions, whereas the calibrated $R_{s,min}$ integrates the influence of canopy organization, foliage orientation, and the complex interaction

https://doi.org/10.5194/egusphere-2026-5685
Preprint. Discussion started: 11 November 2026
© Author(s) 2026. CC BY 4.0 License.

between stomatal and non-stomatal pathways. Non-stomatal uptake can contribute substantially to O_3 deposition and may obscure physiological signals under specific meteorological conditions (Zhang et al., 2002). Moreover, the multiplicative stomatal response functions used in the present inversion simplify the interactions among radiation, temperature, atmospheric humidity, and plant physiological activity. Comparisons of multiplicative and photosynthesis-based deposition schemes have shown that the representation of stomatal regulation can alter simulated O_3 uptake and its response to environmental change (Sun et al., 2022). This suggests that while stomatal control is an important component of canopy O_3 uptake, its expression is frequently constrained or modified by the structural and aerodynamic conditions of urban vegetation.

4.3 Coupled structural, aerodynamic, and physiological controls on O_3 deposition

The sensitivity analysis revealed substantial differences in the response of model-estimated Vd to structural and environmental input parameters. The sensitivity ranking of $LAI > u > z_0 > LAD \approx T$ suggests that canopy structural and aerodynamic parameters strongly influence Vd estimates within the modified-gradient framework (Massman, 1997). The high stability of *LAI* sensitivity throughout the diurnal cycle, contrasted with the transient impacts of wind speed and temperature, indicates a more consistent model response to *LAI* perturbations than to the tested meteorological parameters. This ranking describes the relative sensitivity of the estimation framework and does not establish the dominance of structural controls over plant physiology in actual deposition.

Within the present sensitivity experiments, a 20% increase in *LAI* reduced model-estimated V_d by 17.55%, whereas a corresponding decrease increased V_d by 21.07%. This negative model response may reflect the representation of canopy-dependent aerodynamic transport, but it does not establish a general inverse relationship between *LAI* and actual O_3 deposition. Increasing *LAI* can expand the surface area available for stomatal and non-stomatal uptake while simultaneously altering wind attenuation, turbulent exchange, radiation penetration, and stomatal activity within the canopy. The

https://doi.org/10.5194/egusphere-2026-5685
Preprint. Discussion started: 11 November 2026
© Author(s) 2026. CC BY 4.0 License.

net deposition response therefore depends on the balance between O_3 supply and surface uptake. Multilayer canopy models explicitly represent these vertical interactions and demonstrate the importance of resolving both atmospheric transport and biological sinks (Zhou et al., 2017). Photosynthesis-based approaches further account for physiological responses to radiation and environmental conditions, linking canopy structure to stomatal uptake (Lei et al., 2020; Sun et al., 2022). The negative *LAI* sensitivity identified here is therefore best interpreted as a property of the current estimation framework under the prescribed parameter perturbations. Independent observations or multilayer simulations would be required to determine whether similar responses occur under realistic changes in canopy density and associated physiological and aerodynamic conditions (Finco et al., 2018; Wesely & Hicks, 2000).

4.4 Limitations and implications

Several constraints in the present study warrant consideration in future research. First, all measurements were conducted under summer clear-sky conditions, representing a specific meteorological window that may not reflect annual averages or deposition behavior under cooler, more humid, or highly turbulent conditions (Baldocchi, 1988; Baldocchi, 2003). Second, despite the application of rigorous aerodynamic screening and wind-direction filtering, the residual effects of building-induced turbulence and background concentration heterogeneity in complex urban settings cannot be completely eliminated (Roth, 2000). The modified-gradient estimates also depend on the assumptions used to represent vertical turbulent exchange, which may introduce uncertainty under heterogeneous urban canopy conditions. Third, the inversion of intrinsic resistance parameters relies on a simplified resistance framework and prescribed environmental response functions, which introduces structural uncertainty into the calibrated values (Zhang et al., 2003). The simultaneous estimation of $R_{s,min}$ and R_{ns} may introduce parameter dependence, while the prescribed stomatal response functions cannot fully represent the interactions among plant physiological activity and environmental conditions. In addition, the sensitivity experiments

https://doi.org/10.5194/egusphere-2026-5685
Preprint. Discussion started: 11 November 2026
© Author(s) 2026. CC BY 4.0 License.

examined individual parameter perturbations with other inputs held constant, without accounting for their potential covariation under natural conditions. Future work should therefore extend these species-resolved observations across full seasonal cycles and a broader range of urban morphologies to test the robustness of the interspecific patterns identified in this study.

The findings of this study offer critical implications for both atmospheric modeling and urban environmental policy. Although the selected species are widely distributed across urban environments (**Figure S6**), their geographical occurrence alone does not establish the transferability of the fitted resistance parameters. These parameters were derived under specific summer meteorological conditions and canopy configurations, and their application to other regions requires evaluation against local physiological, structural, and aerodynamic conditions. The identified interspecific heterogeneity suggests that current regional air-quality models, which typically aggregate urban vegetation into coarse land-cover categories, may not fully represent the street-scale variability of O_3 removal (Grote et al., 2016). The species-resolved resistance estimates and structural characteristics derived here provide observational constraints for evaluating more differentiated vegetation representations in regional air-quality models, although their effects on model performance remain to be tested (Wu et al., 2015). At the management level, these results support the consideration of both canopy structure and physiological characteristics in urban greening assessments. Specifically, species differences in deposition velocity and flux suggest that canopy structure, atmospheric transport, and physiological uptake should be evaluated jointly rather than relying on individual traits such as *LAI* or stomatal conductance alone (Clifton et al., 2020). Further evaluation across contrasting urban environments would help determine the applicability of these species-level parameters to atmospheric modeling and vegetation management.

5. Conclusions

This study quantified O_3 dry deposition across 20 common urban tree species in

https://doi.org/10.5194/egusphere-2026-5685
Preprint. Discussion started: 11 November 2026
© Author(s) 2026. CC BY 4.0 License.

Hangzhou using a modified micrometeorological gradient method and resistance-based inversion. Substantial interspecific differences were observed in deposition characteristics and inferred resistance parameters. Platanus acerifolia exhibited the largest vertical O_3 concentration gradient (10.02 ± 0.86 ppb), while Liriodendron chinense and Magnolia grandiflora showed the highest mean daytime deposition velocity (0.890 ± 0.026 cm s^{-1}) and flux (0.382 ± 0.022 μg m^{-2} s^{-1}), respectively. Standardized stomatal conductance was positively correlated with inverted minimum stomatal resistance (R^2 = 0.36, P < 0.001), indicating a physiological contribution to interspecific variation. Sensitivity analysis identified LAI, wind speed, and roughness length as the most influential inputs within the estimation framework, with a 20% increase in LAI reducing estimated deposition velocity by 17.55%.

These findings demonstrate that species-level variation in O_3 deposition cannot be fully characterized by stomatal properties or canopy structure alone, but reflects the coupling of physiological uptake and aerodynamic transport. Compared with conventional land-cover-based parameterizations, the species-resolved observations and resistance estimates provide a more differentiated characterization of urban vegetation. However, the negative *LAI* response reflects model sensitivity rather than an independently established deposition mechanism, while the summer-only observations and resistance inversion assumptions limit parameter transferability. Further validation across seasons and urban environments is needed before applying these estimates more broadly in atmospheric deposition models.

Data availability

Data will be made available on request.

Supporting Information

Relationship between LAD and tree height (**Section S1**); in-situ ozone dry deposition observation systems (**Section S2**); ozone dry deposition calculation (**Section S3**); resistance-based inversion of stomatal and non-stomatal parameters (**Section S4**);

https://doi.org/10.5194/egusphere-2026-5685
Preprint. Discussion started: 11 November 2026
© Author(s) 2026. CC BY 4.0 License.

dendrometric traits and functional groups of the 20 studied tree species (**Table S1**); idealized LAD vertical profiles for conical, umbrella-shaped, spherical, and cylindrical crowns (**Figures S1–S4**); field configurations of the in-situ ozone dry deposition observation systems and mobile platforms (**Figure S5**); and species geographic distribution maps across China indicating regional and global generalizability (**Figure S6**).

Acknowledgements

The author's work was supported by the National Natural Science Foundation of China [grant number 32672474, 32572143, 32101573], and the Zhejiang Provincial Natural Science Foundation of China [grant number LZJMY25D050005].

References

Baldocchi, D.: A multi-layer model for estimating sulfur dioxide deposition to a deciduous oak forest canopy, Atmos. Environ., 22, 869–884, https://doi.org/10.1016/0004-6981(88)90264-8, **1988**.

Baldocchi, D. D.: Assessing the eddy covariance technique for evaluating carbon dioxide exchange rates of ecosystems: past, present and future, Global Change Biol., 9, 479–492, https://doi.org/10.1046/j.1365-2486.2003.00629.x, **2003**.

Baklanov, A., Hänninen, O., Slördal, L. H., et al.: Integrated systems for forecasting urban meteorology, air pollution and population exposure, Atmos. Chem. Phys., 7, 855–874, https://doi.org/10.5194/acp-7-855-2007, **2007**.

Britter, R. E., and Hanna, S. R.: Flow and dispersion in urban areas, Annu. Rev. Fluid Mech., 35, 469–496, https://doi.org/10.1146/annurev.fluid.35.101101.161147, **2003**.

Büker, P., Emberson, L. D., Ashmore, M. R., et al.: Comparison of different stomatal conductance algorithms for ozone flux modelling, Environ. Pollut., 146, 726–735,

https://doi.org/10.5194/egusphere-2026-5685
Preprint. Discussion started: 11 November 2026
© Author(s) 2026. CC BY 4.0 License.



https://doi.org/10.1016/j.envpol.2006.04.007, **2007**.

Clifton, O. E., Fiore, A. M., et al.: Dry deposition of ozone over land: processes, measurement, and modeling, Rev. Geophys., 58, e2019RG000670, https://doi.org/10.1029/2019RG000670, **2020**.

Dong, W., Ma, D., Zhang, M., et al.: Spatial heterogeneity of biogenic VOC emissions and their potential contribution to secondary air pollution in three Chinese megacities: an exploratory assessment, Urban For. Urban Green., 119, 129385, https://doi.org/10.1016/j.ufug.2026.129385, **2026**.

Emberson, L., Ashmore, M. R., Cambridge, H. M., et al.: Modelling stomatal ozone flux across Europe, Environ. Pollut., 109, 403–413, https://doi.org/10.1016/S0269-7491(00)00043-9, **2000**.

Fares, S., Conte, A., Alivernini, A., et al.: Testing removal of carbon dioxide, ozone, and atmospheric particles by urban parks in Italy, Environ. Sci. Technol., 54, 14910–14922, https://doi.org/10.1021/acs.est.0c04740, **2020**.

Fitzky, A. C., Sandén, H., Karl, T., et al.: The interplay between ozone and urban vegetation—BVOC emissions, ozone deposition, and tree ecophysiology, Front. For. Glob. Change, 2, 50, https://doi.org/10.3389/ffgc.2019.00050, **2019**.

Finco, A., Coyle, M., Nemitz, E., et al.: Characterization of ozone deposition to a mixed oak–hornbeam forest—flux measurements at five levels above and inside the canopy and their interactions with nitric oxide, Atmos. Chem. Phys., 18, 17945–17961, https://doi.org/10.5194/acp-18-17945-2018, **2018**.

Fleming, Z. L., Doherty, R. M., von Schneidemesser, E., et al.: Tropospheric Ozone Assessment Report: Present-day ozone distribution and trends relevant to human health, Elem. Sci. Anth., 6, 12, https://doi.org/10.1525/elementa.273, **2018**.

Fowler, D., Pilegaard, K., Sutton, M. A., et al.: Atmospheric composition change: ecosystems–atmosphere interactions, Atmos. Environ., 43, 5193–5267, https://doi.org/10.1016/j.atmosenv.2009.07.068, **2009**.

Gaur, R., and Singh, H.: Urban tree responses to climate change and environmental pollution, in: Urban Forests, Climate Change and Environmental Pollution:

https://doi.org/10.5194/egusphere-2026-5685
Preprint. Discussion started: 11 November 2026
© Author(s) 2026. CC BY 4.0 License.



592 Physio-Biochemical and Molecular Perspectives to Enhance Urban Resilience,
593 279–305, https://doi.org/10.1007/978-3-031-67837-0_14, **2024**.
594 Grote, R., Samson, R., Alonso, R., et al.: Functional traits of urban trees: air pollution
595 mitigation potential, Front. Ecol. Environ., 14, 543–550,
596 https://doi.org/10.1002/fee.1426, **2016**.
597 Karl, T., Harley, P., Emmons, L., et al.: Efficient atmospheric cleansing of oxidized
598 organic trace gases by vegetation, Science, 330, 816–819,
599 https://doi.org/10.1126/science.1192534, **2010**.
600 Kim, G., Lee, J., Lee, M. I., et al.: Impacts of urbanization on atmospheric circulation
601 and aerosol transport in a coastal environment simulated by the WRF-Chem
602 coupled with urban canopy model, Atmos. Environ., 249, 118253,
603 https://doi.org/10.1016/j.atmosenv.2021.118253, **2021**.
604 Körner, C.: Leaf diffusive conductances in the major vegetation types of the globe, in:
605 Ecophysiology of Photosynthesis, 100, 463–490, https://doi.org/10.1007/978-3-
606 642-79354-7_22, **1995**.
607 Lei, Y., Yue, X., Liao, H., Gong, C., and Zhang, L.: Implementation of Yale Interactive
608 terrestrial Biosphere model v1.0 into GEOS-Chem v12.0.0: a tool for biosphere–
609 chemistry interactions, Geosci. Model Dev., 13, 1137–1153,
610 https://doi.org/10.5194/gmd-13-1137-2020, **2020**.
611 Li, K., Jacob, D. J., Liao, H., et al.: Anthropogenic drivers of 2013–2017 trends in
612 summer surface ozone in China, Proc. Natl. Acad. Sci. USA, 116, 422–427,
613 https://doi.org/10.1073/pnas.1812168116, **2019**.
614 Lin, M., Malyshev, S., Shevliakova, E., et al.: Sensitivity of ozone dry deposition to
615 ecosystem–atmosphere interactions: a critical appraisal of observations and
616 simulations, Global Biogeochem. Cycles, 33, 1264–1288,
617 https://doi.org/10.1029/2018GB006157, **2019**.
618 Massman, W.: An analytical one-dimensional model of momentum transfer by
619 vegetation of arbitrary structure, Boundary-Layer Meteorol., 83, 407–421,
620 https://doi.org/10.1023/A:1000234813011, **1997**.

https://doi.org/10.5194/egusphere-2026-5685
Preprint. Discussion started: 11 November 2026
© Author(s) 2026. CC BY 4.0 License.



Manes, F., and Salvatori, E.: Ecosystem services of urban trees: the case of Rome, Agrochimica, 58, 222–233, https://doi.org/10.12871/0021857201436, **2014**.

Medlyn, B. E., Duursma, R. A., Eamus, D., et al.: Reconciling the optimal and empirical approaches to modelling stomatal conductance, Global Change Biol., 17, 2134–2144, https://doi.org/10.1111/j.1365-2486.2010.02375.x, **2011**.

Monks, P. S., Archibald, A. T., Colette, A., et al.: Tropospheric ozone and its precursors from the urban to the global scale from air quality to short-lived climate forcer, Atmos. Chem. Phys., 15, 8889–8973, https://doi.org/10.5194/acp-15-8889-2015, **2015**.

Nowak, D. J., and Greenfield, E. J.: US urban forest statistics, values, and projections, J. For., 116, 164–177, https://doi.org/10.1093/jofore/fvx004, **2018**.

Ren, Y., Qu, Z., Du, Y., et al.: Air quality and health effects of biogenic volatile organic compounds emissions from urban green spaces and the mitigation strategies, Environ. Pollut., 230, 849–861, https://doi.org/10.1016/j.envpol.2017.06.049, **2017**.

Ren, Y., Ge, Y., Gu, B., et al.: Role of management strategies and environmental factors in determining the emissions of biogenic volatile organic compounds from urban greenspaces, Environ. Sci. Technol., 48, 6237–6246, https://doi.org/10.1021/es4054434, **2014**.

Roth, M.: Review of atmospheric turbulence over cities, Q. J. R. Meteorol. Soc., 126, 941–990, https://doi.org/10.1002/qj.49712656409, **2000**.

Schmid, H. P.: Footprint modeling for vegetation atmosphere exchange studies: a review and perspective, Agric. For. Meteorol., 113, 159–183, https://doi.org/10.1016/S0168-1923(02)00107-7, **2002**.

Sicard, P., Agathokleous, E., Araminiene, V., et al.: Should we see urban trees as effective solutions to reduce increasing ozone levels in cities?, Environ. Pollut., 243, 163–176, https://doi.org/10.1016/j.envpol.2018.08.049, **2018**.

Stein, A., Gerstner, K., and Kreft, H.: Environmental heterogeneity as a universal driver of species richness across taxa, biomes and spatial scales, Ecol. Lett., 17, 866–880,

https://doi.org/10.5194/egusphere-2026-5685
Preprint. Discussion started: 11 November 2026
© Author(s) 2026. CC BY 4.0 License.



https://doi.org/10.1111/ele.12277, **2014**.

Sun, S., Tai, A. P. K., Yung, D. H. Y., Wong, A. Y. H., Ducker, J. A., and Holmes, C. D.: Influence of plant ecophysiology on ozone dry deposition: comparing between multiplicative and photosynthesis-based dry deposition schemes and their responses to rising CO_2 level, Biogeosciences, 19, 1753–1776, https://doi.org/10.5194/bg-19-1753-2022, **2022**.

Wang, H., Liu, Z., Zhang, Y., et al.: Impact of different urban canopy models on air quality simulation in Chengdu, southwestern China, Atmos. Environ., 267, 118775, https://doi.org/10.1016/j.atmosenv.2021.118775, **2021**.

Wesely, M. L., Doskey, P. V., and Shannon, J. D.: Deposition parameterizations for the Industrial Source Complex (ISC3) model, ANL/ER/TR-01/003, Argonne National Laboratory, Environmental Research Division, Argonne, IL, USA, 128 pp., https://doi.org/10.2172/1260839, **2002**.

Wesely, M. L.: Parameterization of surface resistances to gaseous dry deposition in regional-scale numerical models, Atmos. Environ., 41, 52–63, https://doi.org/10.1016/j.atmosenv.2007.10.058, **2007**.

Wu, Z. Y., Zhang, L., Wang, X. M., et al.: A modified micrometeorological gradient method for estimating O_3 dry depositions over a forest canopy, Atmos. Chem. Phys., 15, 7487–7496, https://doi.org/10.5194/acp-15-7487-2015, **2015**.

Wesely, M., and Hicks, B.: A review of the current status of knowledge on dry deposition, Atmos. Environ., 34, 2261–2287, https://doi.org/10.1016/S1352-2310(99)00467-7, 2000.

Xu, J., Huang, X., Wang, N., et al.: Understanding ozone pollution in the Yangtze River Delta of eastern China from the perspective of diurnal cycles, Sci. Total Environ., 752, 141928, https://doi.org/10.1016/j.scitotenv.2020.141928, **2021**.

Zhang, L., Brook, J. R., and Vet, R.: On ozone dry deposition—with emphasis on non-stomatal uptake and wet canopies, Atmos. Environ., 36, 4787–4799, https://doi.org/10.1016/S1352-2310(02)00567-8, **2002**.

Zhang, L., Brook, J. R., and Vet, R.: A revised parameterization for gaseous dry deposition in air-quality models, Atmos. Chem. Phys., 3, 2067–2082,

https://doi.org/10.5194/egusphere-2026-5685
Preprint. Discussion started: 11 November 2026
© Author(s) 2026. CC BY 4.0 License.



https://doi.org/10.5194/acp-3-2067-2003, **2003**.

Zhou, P., Ganzeveld, L., Rannik, Ü., Zhou, L., Gierens, R., Taipale, D., Mammarella, I., and Boy, M.: Simulating ozone dry deposition at a boreal forest with a multi-layer canopy deposition model, Atmos. Chem. Phys., 17, 1361–1379, https://doi.org/10.5194/acp-17-1361-2017, **2017**.